# Density of critical clusters in strips of strongly disordered systems

M. Karsai,[1,2] I. A. Kovács,[3,4] J-Ch. Anglès d'Auriac,[2] and F. Iglói[3,1]
[1]*Institute of Theoretical Physics, Szeged University, H-6720 Szeged, Hungary*
[2]*Institut Néel-MCBT CNRS, Boîte Postale 166, F-38042 Grenoble, France*
[3]*Research Institute for Solid State Physics and Optics, H-1525 Budapest, P. O. Box 49, Hungary*
[4]*Department of Physics, Loránd Eötvös University, H-1117 Budapest, Pázmány P. s. 1/A, Hungary*
(Received 9 May 2008; revised manuscript received 3 September 2008; published 11 December 2008)

We consider two models with disorder-dominated critical points and study the distribution of clusters that are confined in strips and touch one or both boundaries. For the classical random bond Potts model in the large-$q$ limit, we study optimal Fortuin-Kasteleyn clusters using a combinatorial optimization algorithm. For the random transverse-field Ising chain, clusters are defined and calculated through the strong-disorder renormalization group method. The numerically calculated density profiles close to the boundaries are shown to follow scaling predictions. For the random bond Potts model, we have obtained accurate numerical estimates for the critical exponents and demonstrated that the density profiles are well described by conformal formulas.

DOI: 10.1103/PhysRevE.78.061109 PACS number(s): 64.60.Bd, 68.18.Jk, 75.10.Nr

## I. INTRODUCTION

### A. Clusters in critical models

In a critical system, the correlation length is divergent and domains of correlated sites appear in all length scales. These correlated domains are most easily visualized for percolation [1], in which they are the connected clusters. In discrete spin models, such as the Ising and Potts models, domains of correlated spins can be identified in different ways. One possibility is to use geometrical clusters [2] (also called Ising or Potts clusters), which are domains of parallel spins. In two dimensions (2D) geometrical clusters percolate throughout the sample at the critical temperature and their fractal dimension can be obtained through conformal invariance [3]. This fractal dimension is generally different from the fractal dimension of Fortuin-Kasteleyn (FK) clusters [4], which are represented by graphs of the high-temperature expansion. From a geometrical cluster, the FK cluster is obtained by removing bonds with a probability $1-p=e^{-K_c}$, $K_c$ being the critical value of the coupling. The fractal dimension of a FK cluster is directly related to the scaling dimension of the magnetization.

In a finite geometry, such as inside strips or squares, one is interested in the spanning probability and different crossing problems of the critical clusters. For 2D percolation many exact and numerical results have been obtained in this field [5–13]. Another interesting problem is the density of clusters in restricted geometries [14], which is defined by the fraction of samples for which a given point belongs to a cluster with some prescribed property, such as touching the edges of infinite and half-infinite strips, squares, etc. This latter problem is analogous to the calculation of order parameter profiles in restricted geometries, which has been intensively studied through conformal invariance and numerical methods [15–29].

### B. Density of critical percolation clusters in strips

Very recently the density of critical percolation clusters has been studied in different 2D restricted geometries and presumably exact expressions are obtained through conformal invariance [14]. Here we recapitulate some of these results, which are valid for an infinite strip of width $L \gg 1$ in the continuum limit, when the position of a point measured perpendicular to the strip is $l \gg 1$ and the scaling variable is $y=l/L=O(1)$. Three different types of densities are calculated.

*Crossing clusters* touch both boundaries of the strip and their density is given by

$$\rho_b(y) \propto (\sin \pi y)^{-x_b}\left[\left(\cos\frac{\pi y}{2}\right)^{x_s}+\left(\sin\frac{\pi y}{2}\right)^{x_s}-1\right], \quad (1)$$

in which $x_b=5/48$ and $x_s=1/3$ are the scaling dimensions of the order parameter (magnetization) and that of the surface order parameter [1], respectively.

If the clusters touch one boundary of the strip, say at $y=l/L\to 0$, irrespective of the other, their density is given by

$$\rho_0(y) \propto (\sin \pi y)^{-x_b}\left(\cos\frac{\pi y}{2}\right)^{x_s}. \quad (2)$$

This density is analogous to the order parameter profile in the system with fixed-free boundary conditions [19,20].

Finally, we consider clusters that are touching the boundary either at $l=1$ or at $l=L$ or both, and their density is given by

$$\rho_e(y) \propto (\sin \pi y)^{-x_b}, \quad (3)$$

which is analogous to the order parameter profile with parallel fixed spin boundary conditions [15]. Note that we have the relation $\rho_b(y)=\rho_0(y)+\rho_1(y)-\rho_e(y)$, with $\rho_1(y)=\rho_0(1-y)$.

The results in Eqs. (1)–(3) are derived for percolation; however, it is expected that they also hold for the densities of FK clusters in 2D conformally invariant systems. Here we refer to the analogous expressions for order parameter profiles, in which case both Eqs. (2) and (3) follow from conformal considerations; thus these are valid for conformally invariant models. On the other hand, the third density $\rho_b(y)$ can be expressed using the two previous ones.

 

### C. Clusters in disordered systems

#### 1. Isotropic models

Correlated clusters are defined also in disordered models, in which the physical observables (magnetization profile, cluster density, etc.) are averaged over quenched disorder, too. In isotropic random systems conformal symmetry is expected to hold at the critical point so that average operator profiles and average cluster densities are expected to be invariant under conformal transformations. Among disordered systems an interesting class is represented by such models in which the transition in the pure version is of first order, but in the disordered version the transition softens to second order [30]. This type of random fixed point can be found, among others, in the two-dimensional random bond Potts model (RBPM) for $q>4$, $q$ being the number of states [31,32].

#### 2. Anisotropic models

If the distribution of the disorder is not isotropic, e.g., it has a layered structure, then the scaling behavior of the disordered system is often anisotropic, too, which is manifested in the fact that the critical clusters have an elongated shape. This means that the characteristic sizes of the clusters parallel, $\xi_{\parallel}$, and perpendicular, $\xi_{\perp}$, to the layers are generally related as $\xi_{\parallel} \sim \xi_{\perp}^{z}$, with an anisotropy exponent $z \neq 1$. These essentially anisotropic models are not conformally invariant. A well-known example in this class is the McCoy-Wu model [33], which is a two-dimensional Ising model with layered disorder. Study of this system, as well as its one-dimensional quantum version, the random transverse-field Ising chain (RTFIC), has shown [34] that the critical behavior is controlled by a so-called infinite-disorder fixed point (IDFP), in which scaling is strongly anisotropic [35]. The characteristic lengths are related as $\ln \xi_{\parallel} \sim \xi_{\perp}^{2}$ so that the anisotropy exponent is formally infinite. The same IDFP is found to control the critical behavior of the randomly layered $q$-state Potts model [36], as well as, for strong enough layered disorder, the critical behavior of percolation [37] and directed percolation [38]. Operator profiles in the RTFIC have been studied numerically [23] and the data obtained could be well fitted by curves which are obtained by analogy to the conformal results.

### D. Aim of the paper

In this paper we study the density of critical clusters in two problems in which the critical properties are dominated by strong-disorder effects. The first model is the two-dimensional RBPM in the large-$q$ limit. In this model for a given realization of disorder the high-temperature series expansion is dominated by a single graph [39], the so-called optimal diagram, which is calculated for each finite sample by a combinatorial optimization algorithm [40]. Clusters in the optimal diagram are isotropic, and the density of clusters is obtained through averaging over disorder realizations. The second model we consider is the RTFIC, i.e., a random quantum model which is related to the classical McCoy-Wu model, in which the Fortuin-Kasteleyn clusters are strongly anisotropic. In the RTFIC, clusters of correlated spins can be defined and calculated by the so-called strong-disorder renormalization group (SDRG) method [35]. During renormalization the system is transformed into a set of effective spin clusters and, for a finite system with a given realization of the disorder, one obtains the final cluster, which contains mostly correlated sites. The fractal dimension of the final cluster at the critical point is directly related to the scaling dimension of the magnetization of the RTFIC. Here we calculate the density of these final clusters, which are confined in a (one-dimensional) strip.

The two models we study in this paper are expected to be closely related, as far as their critical properties are concerned. Based on numerical and analytical studies [41,42], the scaling dimension of the magnetization, $x_b$, and that of the surface magnetization, $x_s$, are conjectured to be the same for both systems and given by [34]

$$x_b = \frac{3-\sqrt{5}}{4}, \quad x_s = \frac{1}{2}. \tag{4}$$

In this paper we calculate the critical densities of both models and compare them with the conformal results in Eqs. (1)–(3).

The structure of the paper is the following. Section II is devoted to the RBPM. Here we define the model, outline the calculation of the optimal diagram, and then analyze the statistics of the distribution of the clusters. The numerically calculated densities are then compared with the conformal formulas. In Sec. III we define the RTFIC, recapitulate the essence of the SDRG method, and then numerically calculate final clusters at the critical point. The numerically calculated densities are compared with analytical formulas in this case, too. The paper is closed with a discussion.

## II. CLUSTERS IN THE OPTIMAL DIAGRAM OF THE RBPM

### A. Model

The $q$-state Potts model [43] is defined by the Hamiltonian

$$\mathcal{H} = -\sum_{\langle i,j \rangle} J_{ij} \delta(\sigma_i, \sigma_j) \tag{5}$$

in terms of the Potts-spin variables $\sigma_i = 0, 1, \ldots, q-1$ at site $i$. The summation runs over all edges of a lattice $\langle i,j \rangle \in E$, and in our study the couplings $J_{ij}>0$ are independent and identically distributed random numbers. To write the partition sum of the system it is convenient to use the random cluster representation [4]:

$$Z = \sum_{G \subseteq E} q^{c(G)} \prod_{ij \in G} (q^{\beta J_{ij}} - 1), \tag{6}$$

where $\beta = 1/(k_B T \ln q)$, the sum runs over all subsets of bonds, $G \subseteq E$, and $c(G)$ stands for the number of connected components of $G$. In the following we restrict ourselves to the square lattice, in which case the phase transition in the nonrandom model is of second order (first order) for $q \leqslant 4$ ($q>4$) [44], but for random couplings the phase transition softens to second order for any value of $q$ [45,46]. For con-

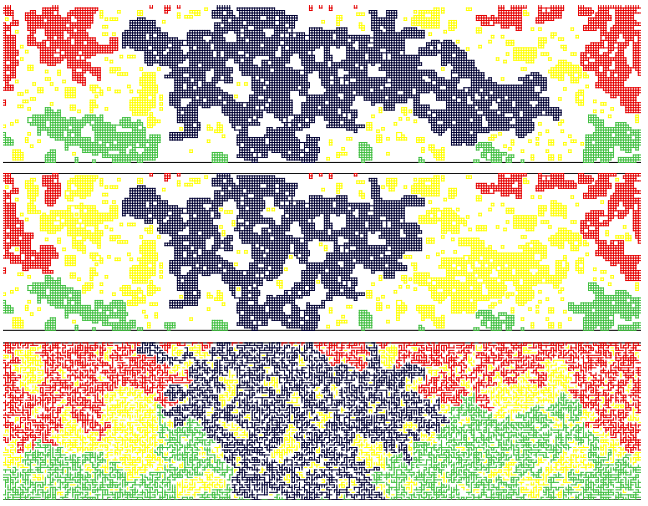

FIG. 1. (Color online) Optimal diagrams of the RBPM for three realizations of the disorder of different strengths. Bottom panel, $\Delta=1/2$, standard bond percolation; middle panel, $\Delta=5/12$; top panel, $\Delta=4/12$. We have used different colors (gray scales) to visualize the different types of clusters in the optimal diagram: spanning clusters (black), clusters that touch only the upper (lower) boundary of the strip [red (green)], and clusters that have no common points with the boundary (yellow). Note that the breaking-up length is increasing with decreasing $\Delta$.

ceptual simplicity we consider the large-$q$ limit, where $q^{\beta J_{ij}} \gg 1$, and the partition function can be written as

$$Z=\sum_{G\subseteq E} q^{\phi(G)}, \quad \phi(G)=c(G)+\beta\sum_{ij\in G} J_{ij}, \tag{7}$$

which is dominated by the largest term, $\phi^*=\max_G \phi(G)$. Consequently at a given temperature disorder fluctuations play a dominant role over thermal fluctuations. The optimal diagram of the RBPM is analogous to the diagram of connected bonds in percolation theory. For example, at the critical point there is a giant cluster in the optimal diagram, the fractal dimension of which, $d_f$, is related to the scaling dimension of the (average) magnetization as $d=d_f+x_b$, where $d=2$ is the dimension of the system. One can also study other questions, such as distribution of the mass of the connected clusters, spanning probability, surface scaling exponent, etc. Here we are going to investigate the density of clusters in strip geometry.

During our study we use a bimodal form of the disorder, when the reduced couplings $K_{ij}=\beta J_{ij}$ take two values, $K_1=K-\Delta$ and $K_2=K+\Delta$, with equal probability. Generally we study the critical point of the system that is located [47] at $K=K_c=1/2$, independently of the value of $0\leqslant\Delta\leqslant 1/2$. Note that the pure system is obtained for $\Delta=0$, whereas for $\Delta=1/2$, when just the strong bonds are present in the system, we have the traditional percolation problem. The evaluation of the optimal diagram with decreasing values of $\Delta$ is shown in Fig. 1. Here one can see that with decreasing $\Delta$ the clusters become more compact. To characterize this effect we define a length scale, the so called breaking-up length $l_b$: in a finite system of linear size $L<l_b$ the optimal diagram is typically homogeneous (either empty or fully connected) and for $L>l_b$ it contains both empty and connected parts. If we want to determine $l_b$, we fix the size of the system, $L$, and for a given distribution of the bonds decrease $\Delta$ until $\Delta_b$, where the optimal set becomes fully connected. Repeating this calculation for several realizations of the disorder, we obtain an average value $\overline{\Delta_b}$, for which the breaking-up length is just $L=l_b$. $l_b$ is a rapidly increasing function of $1/\Delta$; for small $\Delta$ it behaves as [42]

$$l_b \approx l_0 \exp\left[A\left(\frac{K}{\Delta}\right)^2\right]. \tag{8}$$

In a numerical calculation on a finite sample, one should have the relation $L\gg l_b$; thus $\Delta$ should be not too small. On the other hand, one should also be sufficiently far from the percolation limit, $\Delta=1/2$, in order to get rid of crossover effects. This means that the optimal choice of $\Delta$ is a result of a compromise, which in our case seems to be around $\Delta=5/12$, when the typical breaking-up length is about $l_b\sim 14$. Most of our studies are made for this value, but in order to check universality, i.e., disorder independence of the results, we have also made a few calculations for $\Delta=21/48$.

Calculation of the optimal diagram for a given realization of disorder is a nontrivial optimization problem, for which a very efficient combinatorial optimization algorithm has been developed [40], which works in strongly polynomial time. Application of this method made it possible to obtain the exact optimal diagram for comparatively large finite systems. In order to have an effective strip geometry, we have considered lattices of rectangular shape with an aspect ratio of 4. The strips have open boundaries along the long direction and a periodic boundary condition was used in the other direction. We mention that the same geometry has been used before for percolation, too [14]. The width of the lattices we considered are from $L=32$ up to 256 (i.e., the largest systems contained 262 144 sites) and for each size we have considered 1000 samples, except for $L=64$ and 128, when we had 1509 and 2128 samples, respectively. These calculations were performed on a cluster of 16 quadricore processors during more than a month.

### B. Densities of critical clusters

We start to study the density of crossing clusters, $\rho_b(l/L)$, the scaling form of which is conjectured in Eq. (1) for conformally invariant systems. For the RBPM the numerically calculated normalized densities $\rho_b(l/L)$ for different widths are shown in Fig. 2. The data for different widths fit the same curve and the finite breaking-up length $l_b$ seems to have only a small effect.

In the surface region $l\ll L$ but $l>l_b$, one expects from scaling theory $\rho_b(l)\sim l^{x_s-x_b}$, which is in accordance with the limiting behavior of the conformal prediction in Eq. (1). In Fig. 3 we have presented $\rho_b(l)$ in a log-log plot in the surface region for the largest finite system. Indeed, for $l>l_b$ the points are well on a straight line, the slope of which is compatible with the conjectured value: $x_s-x_b=0.309$. We have also estimated the asymptotic slope of the curve by drawing a straight line through the points in a window $[l_b+l/2,\ l_b+3l/2]$ by a least squares fit. Fixing $l_b=15$, the estimates

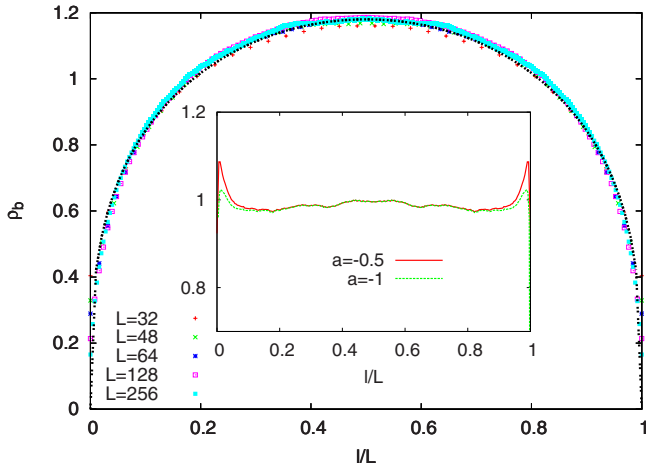


FIG. 2. (Color online) Normalized density profiles $\rho_b(l/L)$ of the RBPM for different widths. The error bars are smaller than the size of the symbols. The dashed line indicates the conformal result in Eq. (1) with the conjectured exponents in Eq. (4) and with the boundary parameter $a=0$ in Eq. (9). In the inset the ratio of simulation to theoretical results is presented for $L=256$ and for two different boundary parameters $a=-0.5$ and $-1.0$ [see Eq. (9)]. The consistency test in Eq. (10) gives $z^2=0.112$ ($a=0.0$), $z^2=0.066$ ($a=-0.5$), and $z^2=0.061$ ($a=-1.0$).

with varying $l$ seem to have $a\sim l^2$ correction (see the inset of Fig. 3) and the extrapolated slope is $x_s-x_b=0.303(8)$, in agreement with the conjectured values in Eq. (4).

We have also checked the conjectured form of the profile in Eq. (1) using the scaling exponents in Eq. (4), which indeed fits very well the scaling curve for the RBPM for the whole profile. We have also calculated the ratio of the simulation to the theoretical results. In this case, following Ref. [14], for the theoretical curve we used the variable

$$y=(l+a)/(L+2a), \tag{9}$$

in which $a=O(1)$ is a free parameter, which measures the effective position of the boundary in the lattice model. By

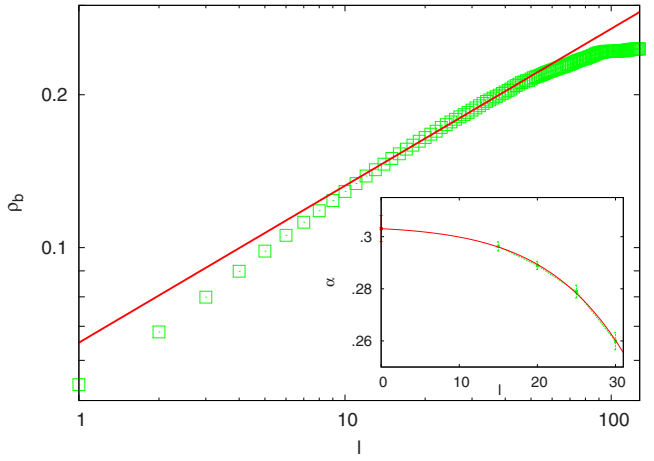


FIG. 3. (Color online) Density profile $\rho_b(l)$ of the RBPM for $L=256$ close to the surface in a log-log plot. The straight (red) line has a slope $x_s-x_b=0.309$. Inset: estimates of the slope using different windows of the fit; see the text. Here the full (red) line indicates a parabolic fit.

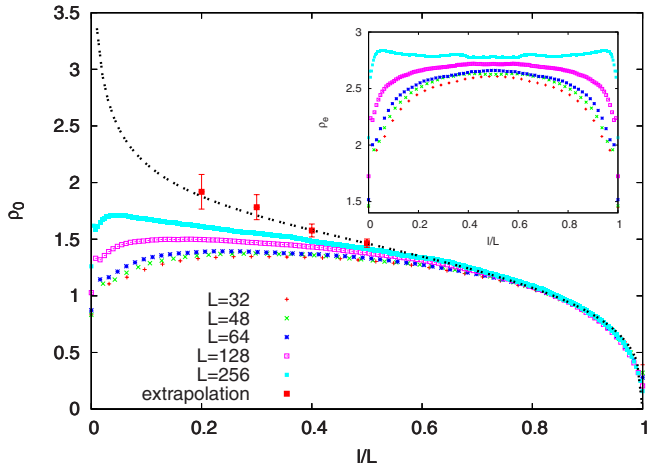


FIG. 4. (Color online) Density profiles $\rho_0(l/L)$ of the RBPM for different widths which approach the same scaling curve at the free boundary $y=1$. The error bars are smaller than the size of the symbols. The extrapolated values for $l/L\geqslant 0.5$ are denoted by red squares. The dashed line indicates the conformal result in Eq. (2) with the conjectured exponents in Eq. (4). Inset: density profiles $\rho_e(l/L)$ for different widths.

varying $a$ from 0 to $-1$ one obtains a better fit in the boundary region, but at the same time the bulk part of the profile remains practically unchanged. As seen in the inset of Fig. 2, in the bulk part of the profile the nonsystematic fluctuation of the ratio around unity is typically 1–2%. Here we have made a consistency check, which is somewhat analogous to the $\chi^2$ test of the distribution of random numbers. We have calculated

$$z^2=\sum_l \frac{[\rho_b(l/L)-\tilde{\rho}_b(l/L)]^2}{\tilde{\rho}_b(l/L)}, \tag{10}$$

where $\rho_b(l/L)$ is the calculated (average) value and $\tilde{\rho}_b(l/L)$ denotes the conjectured result. Indeed $z^2$ is smaller for $a=-0.5$ and $-1.0$ than for $a=0$.

Second, we consider the density of those clusters which are touching one boundary of the strip, $\rho_0(l/L)$, the scaling form of which is conjectured in Eq. (2). This density is analogous to the order parameter profile in the system with fixed-free boundary conditions [19,20]. The numerically calculated densities are shown in Fig. 4 for different widths. The profiles at the fixed boundary, $y=0$, are perturbed by surface effects, which are due to the presence of the finite breaking-up length. Indeed, in terms of the scaled variable $y=l/L$, the size of the perturbed surface region, $\tilde{y}_L$, is a decreasing function of $L$. On the other hand, at the free boundary $y=1$, where the profiles are not perturbed by the fixed surface, the densities approach the same scaling curve, which in the vicinity of the boundary behaves as $\rho_0(y)\sim(1-y)^{x_s-x_b}$. Comparing the scaling curve with the conformal prediction in Eq. (2), we obtain an overall good agreement for $1\geqslant y>0.5$. In the region $y\leqslant 0.5$, where the finite-size profiles deviate more strongly from each other, we used an extrapolation procedure. At a fixed $y$ we have plotted $\rho_0(y)$ as a function of $1/L$ and from this we have estimated

the value of the scaled curve as $L\to\infty$. With this method we have obtained estimates in the region $y\geqslant 0.2$, which are in agreement with the conformal result as seen in Fig. 4.

Turning back to the finite-size dependence of the densities at the fixed surface $y=0$, we note that in the continuum limit $l_b \ll l \ll L$, the scaling form of the density is described by the result of Fisher and de Gennes [48]: $\rho_0(l)\sim l^{-x_b}$. However, on approaching the breaking-up length $l_b$, the increase of the profile is stopped and for $l<l_b$ $\rho_0(l)$ starts to decrease. This is due to the structure of the connected clusters close to the surface. As seen in Fig. 1 the number of touching sites in a cluster is comparatively smaller for the RBPM with $\Delta<1/2$ (top and middle panels of Fig. 1) than for percolation with $\Delta=1/2$ (bottom panel of Fig. 1). Also, for finite widths the small and medium-size touching clusters are rarely represented for the RBPM. As $l$ approaches the other, free side of the strip, the crossing clusters start to bring the dominant contribution to the density $\rho_0(l/L)$, which is then well described by the conformal formula.

Finally, we consider the density of points in clusters that are touching the boundary either at $l=1$ or at $l=L$ or both, which is denoted by $\rho_e(l/L)$, and the conjectured conformal formula is given in Eq. (3). This density is analogous to the order parameter profile with parallel fixed spin boundary conditions [15].

For the RBPM this density is strongly perturbed by the finite breaking-up length at both boundaries, as can be seen in the inset of Fig. 4. In this case we did not try to perform an extrapolation, and conclude that even larger finite systems would be necessary to test the conformal predictions in a direct calculation. In order to try to test the result in Eq. (3), we studied another density which is defined on crossing clusters, so that one expects it to be represented correctly in smaller systems, too. Here we define a density $\rho_e^{\text{line}}(l/L)$ in crossing clusters and consider points only on vertical lines such that at both ends of the given line the cluster touches the boundaries. Since $\rho_e^{\text{line}}(l/L)$ is related to the operator profile with fixed-fixed boundary conditions, we expect that it has the same scaling form as the previously defined density $\rho_e(l/L)$. In Fig. 5 we show the calculated densities for the RBPM, which is compared with the analytical prediction in Eq. (3). A similar analysis for percolation is shown in the inset of Fig. 5. In both cases we found that the numerical and analytical results for this type of profile are in satisfactory agreement, although the statistics of the numerical data is somewhat low, since just a fraction of $\sim L^{-2x_s}\sim L^{-1}$ lines can be used in this analysis. (The nonsystematic fluctuation of the numerical data is less than 1% for percolation and about 3% for the RBPM.)

We can thus conclude that all the critical densities we considered for the RBPM are found in agreement with the conformal predictions in Eqs. (1)–(3), in which we have used the scaling dimensions of the RBPM in Eq. (4). From an analysis of the profile $\rho_b(l)$ close to the boundary we have obtained an accurate estimate of the critical exponent $x_s-x_b$, giving further support to the conjecture in Eq. (4).

## III. FINAL CLUSTERS IN THE RTFIC

### A. Model

The random transverse-field Ising chain is defined by the Hamiltonian

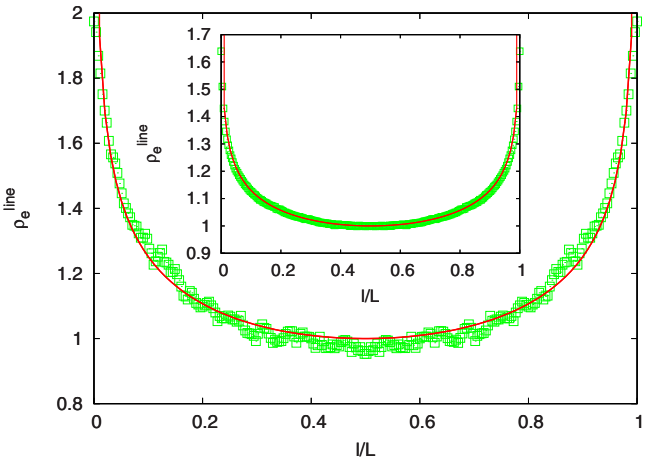


FIG. 5. (Color online) Density profile along a vertical line with two touching boundary points, $\rho_e^{\text{line}}(l/L)$, for the RBPM for $L=256$. The solid (red) curve indicates the conformal result in Eq. (3) with the conjectured exponents in Eq. (4). In the inset the same quantity is shown for percolation. Here in the analytical formula in Eq. (3) we use $x_b=5/48$ and $x_s=1/3$. In both figures the boundary parameter in Eq. (9) is $a=0$.

$$\hat{\mathcal{H}} = -\sum_i J_i \sigma_i^x \sigma_{i+1}^x - \sum_i h_i \sigma_i^z \tag{11}$$

in terms of the Pauli matrices $\sigma_i^{x,z}$ at site $i$. The couplings $J_i$ and the transverse fields $h_i$ are independent random numbers which are taken from the distributions $p(J)$ and $q(h)$, respectively. The critical point of the system is located at $[\ln h]_{\text{av}}=[\ln J]_{\text{av}}$, where we use the notation $[\cdots]_{\text{av}}$ to indicate the average over quenched disorder.

We note that the RTFIC is the Hamiltonian version [49] of the McCoy-Wu model [33], which is a 2D Ising model with layered disorder. In the $i$th layer of this model the couplings in the vertical and horizontal directions are given by $K_1(i)$ and $K_2(i)$, respectively, which are related to the parameters of the RTFIC as $h_i=-\tau^{-1}\tanh^{-1}\exp[-2K_1(i)]$ and $J_i=-\tau^{-1}K_2(i)$, where in the Hamiltonian limit $\tau\to 0$.

### B. SDRG method

The RTFIC can be efficiently studied within the frame of a renormalization group approach [35,50], which is expected to lead to asymptotically exact results [34]. The basic feature of this procedure is to successively eliminate those degrees of freedom that have the largest local energy scale and thus represent the fastest local mode. At a given step of the renormalization, the global energy scale is defined by $\Omega=\max\{J_i,h_i\}$, and the local term of value $\Omega$ is eliminated from the Hamiltonian. Here we have two different elementary renormalization steps: cluster formation and cluster decimation.

*(i) Cluster formation*. If the largest local parameter is a coupling, say $J_2\gg h_2,h_3$ ($h_2$ and $h_3$ being the transverse fields acting at the two ends of $J_2$), then a new spin cluster is formed in an effective transverse field $\tilde{h}_{23}\approx h_2h_3/J_2$, which is calculated in a second-order perturbational calculation. The moment of the new cluster is given by $\tilde{\mu}_{23}=\mu_2+\mu_3$, in

terms of the moments of the original clusters, $\mu_2$ and $\mu_3$. In the starting Hamiltonian all spins have the same moment of unity.

*(ii) Cluster decimation*. If the largest local parameter is a transverse field, say $h_2 \gg J_2, J_3$ ($J_2$ and $J_3$ being the couplings which are connected to the site with $h_2$), then the spin cluster is decimated out and an effective coupling $\tilde{J}_{23} \approx J_2 J_3 / h_2$ is formed between the remaining sites. If the decimated spin is at the boundary of an open chain no new couplings are formed.

During renormalization, we repeat the elementary decimation steps, which at the starting period are only approximate (since the relations $J_2 \gg h_2, h_3$ or $h_2 \gg J_2, J_3$ are not always satisfied), but as the energy scale is reduced and the fixed point $\Omega^* = 0$ is approached (which is valid in the thermodynamic limit), they become asymptotically exact. At this infinite-disorder fixed point the renormalization group equations can be solved analytically. The length scale of the clusters (and bonds), defined by the linear size of the original region which is renormalized to the new variable, is shown [34] to scale as

$$\ell \sim \ln(\Omega/\Omega_0)^2, \tag{12}$$

where $\Omega_0$ is a reference energy scale. On the other hand the average cluster moment behaves as [34]

$$\mu \sim \ln(\Omega/\Omega_0)^{\Phi}, \quad \Phi = \frac{1+\sqrt{5}}{2}. \tag{13}$$

Note that the average magnetization at the critical point behaves as $m(\ell) \sim \mu / \ell \sim \ell^{-x_b}$ as lengths are rescaled by a factor $\ell$, and $x_b = 1 - \Phi/2$ is just the scaling dimension introduced in Eq. (4).

### C. Densities of critical clusters

Here we consider finite chains of length $L$, for which the decimation procedure is stopped after $L-1$ steps and we are left with a single renormalized site. This renormalized site can be represented in terms of the original spins, among which several are decimated out and there are some which are still active; these active spins form the so-called final cluster. The typical moment of this final cluster (i.e., the number of active spins) is $\mu(L) \sim L^{\Phi/2}$. Sites in the final cluster are very strongly correlated, and we can ask questions about the density of sites in the final cluster, i.e., about the probability that a given site is contained in a final cluster. The structure of spins in the final clusters is illustrated in Fig. 6. Note that the final cluster in the 1D space is disconnected, and the correlations are of quantum origin, so that spins in the final cluster flip coherently in time. Densities of critical clusters in the RTFIC are studied numerically. We have considered a large number $(3 \times 10^7)$ of chains of length $L = 2^{13} = 8192$ with open boundary conditions. We used the same type of uniform disorder, $p(J) = q(h) = 1$, for $0 \leqslant J, h \leqslant 1$ and $p(J) = q(h) = 0$, for $J, h > 1$, for both the couplings and the transverse fields; in this way we have satisfied the criticality condition. The strong-disorder renormalization procedure is performed for each chain up to the final renormalized spin,

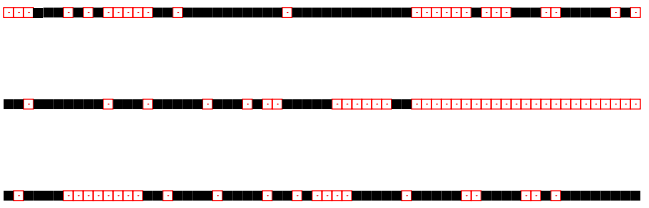

FIG. 6. (Color online) Examples of final clusters in the RTFIC for $L=64$. Nondecimated (i.e., active) spins in the final cluster are denoted by black squares. Top panel, final cluster in general position; middle panel, final cluster containing the boundary spin at $\ell = 1$; bottom panel, final cluster containing both boundary spins at $\ell = 1$ and at $\ell = L$.

and then the statistics of the sites belonging to the final clusters are investigated.

We have studied the density of three different classes of clusters, which have somewhat analogous definitions to the clusters studied for the RBPM. In terms of all final clusters (see the top panel of Fig. 6) we define $\hat{\rho}(l/L)$. If we consider those final clusters which have the boundary point $l=1$ (see the middle panel of Fig. 6) we obtain $\hat{\rho}_0(l/L)$. Finally, if the clusters contain both boundary points $l=1$ and $L$ (see the bottom panel of Fig. 6) we define $\hat{\rho}_{01}(l/L)$. We note that for these densities no analytical conjecture is available, since the system is not conformally invariant.

The density of all final clusters is shown in Fig. 7. First we note that close to the boundaries the behavior of the profile is predicted by scaling theory as $\hat{\rho}(y) \sim y^{x_s - x_b}$, $y \ll 1$, or $\hat{\rho}(\ell) \sim \ell^{x_s - x_b}$, $\ell \ll L$. This relation is indeed satisfied as shown in inset (a) of Fig. 7. From this inset we can see that the microscopic length scale of the model, $l_m$, is just a few lattice spacings and for $l > l_m$ the calculated profile is well described by the asymptotic scaling result. The scaling result is valid for the formula in Eq. (1) with the appropriate scaling dimen-

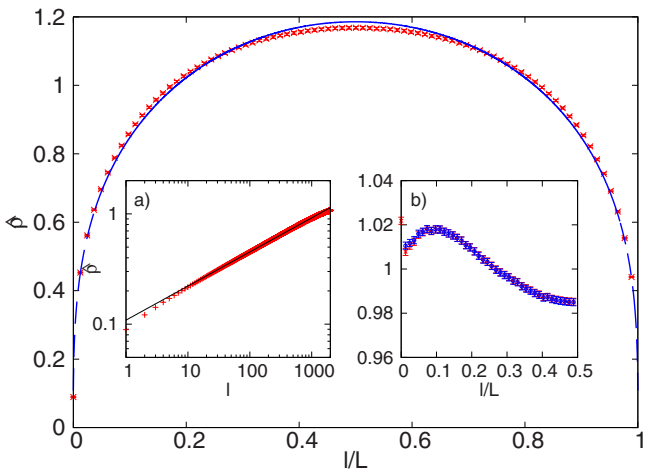


FIG. 7. (Color online) Density profile of the RTFIC considering all final clusters of the SDRG procedure. The dashed (blue) line indicates the formula in Eq. (1). Insets: (a) Density profile close to the surface in a log-log plot. The straight (black) line has a slope $x_s - x_b = 0.309$. (b) Ratio of the numerical results and the formula in Eq. (1). The parameter in Eq. (9) is $a=0$ (red cross) and $a-1$ (blue circle).

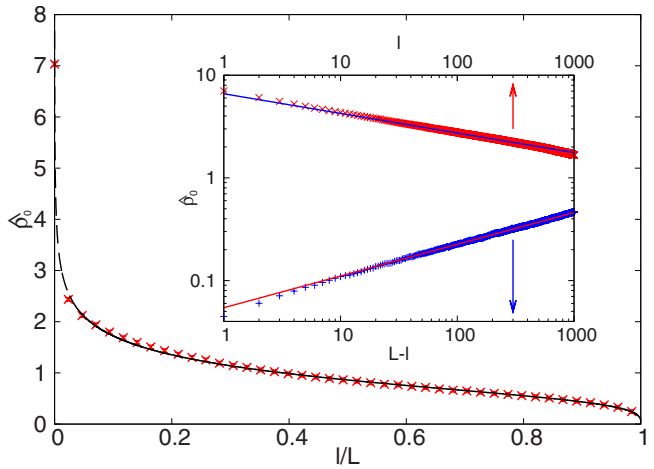


FIG. 8. (Color online) Density profile of the RTFIC considering those final clusters of the SDRG procedure which contain the site at $l=1$. The dashed line indicates the formula in Eq. (14). Inset: density profiles at the two surfaces in a log-log plot. The straight lines have slopes $-x_b=-0.191$ (upper or red) and $x_s-x_b=0.309$ (lower or blue).

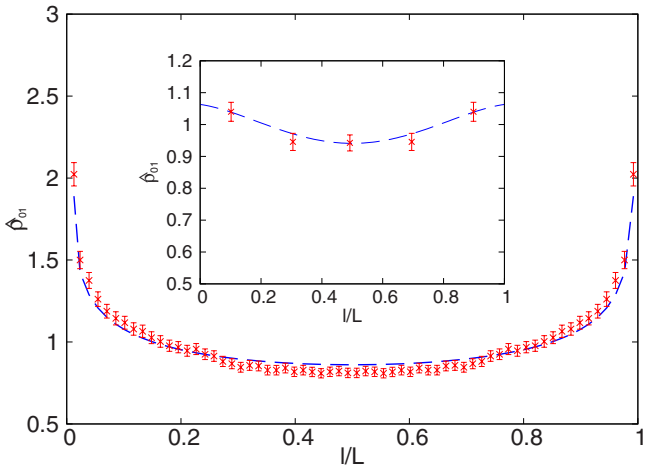


FIG. 9. (Color online) Density profile of the RTFIC considering those final clusters of the SDRG procedure which contain both boundary sites. The dashed line indicates the formula in Eq. (3). Inset: ratio of the numerical results and the formula in Eq. (3). Typical error bars are also indicated.

sions; therefore we tried to compare it with the numerical results. As seen in Fig. 7, the agreement is very good for all values of $y$. To have a more precise check, in inset (b) of Fig. 7 we have presented the ratio of the numerical results and the formula in Eq. (1). Here one can notice small deviations from unity, which are of the order of 1%. Consequently, the formula in Eq. (1) is a very good fit; however, presumably it is not exact.

The density of final clusters which contain the boundary site at $l=1$ is shown in Fig. 8. From scaling theory one knows the behavior of the profile close to the boundaries: $\hat{\rho}_0(y)\sim(y)^{-x_b}$, $y\ll 1$ [or $\hat{\rho}_0(\ell)\sim(\ell)^{-x_b}$, $\ell\ll L$] and $\hat{\rho}_0(y)\sim(1-y)^{x_s-x_b}$, $1-y\ll 1$ [or $\hat{\rho}_0(L-\ell)\sim(L-\ell)^{x_s-x_b}$, $L-\ell\ll L$], respectively. This behavior is indeed found in the numerically calculated profile as seen in the inset of Fig. 8. The asymptotics mentioned above is valid for the formula in Eq. (2). We tried to fit the numerical results with this formula (with the appropriate scaling dimensions); however, the weight of the tail at $y\sim 1$ given by this formula is too large, by about a factor of 2. Much better agreement with the data can be obtained with the formula

$$\hat{\rho}_0(y)\propto(\sin\pi y)^{-x_b}\left[\left(\cos\frac{\pi y}{2}\right)^{x_s}-\left(\sin\frac{\pi y}{2}\right)^{x_s}+1\right], \tag{14}$$

which is just the average of the density of clusters which touch one boundary and may and may not touch the other boundary. As seen in Fig. 8, the analytical and numerical results are close to each other for all $y$, although the agreement is certainly not perfect.

Finally we consider those final clusters that touch both boundaries. The corresponding density $\hat{\rho}_{01}(y)$ is similar to the order parameter profile with fixed-fixed boundary condition and its functional form for percolation is given in Eq. (3). The numerically calculated profile is given in Fig. 9. Here the comparatively large fluctuations of the data points are due to the fact that only a fraction $\sim L^{-2x_s}\sim L^{-1}$ of the samples have a final cluster which touches both boundaries. We have compared the calculated profile with the analytical formula in Eq. (3) using $x_b$ from Eq. (4). The agreement is generally very good, but not fully perfect. Small deviations of the order of a few percent can be observed (see the inset of Fig. 9).

## IV. DISCUSSION

In this paper, we have studied the density of critical clusters in two models the critical properties of which are dominated by disorder effects. Our study is motivated by a recent investigation about ordinary percolation in Ref. [14] in which the densities are calculated in the continuum approximation through conformal invariance. Here we have suggested the generalization of these analytical results for another conformally invariant systems in Eqs. (1)–(3). To test these predictions we have studied numerically the density of FK clusters in infinite strips of the two-dimensional random bond Potts model in the large-$q$ limit. This model is expected to be conformally invariant, which means that average quantities that are related to FK clusters (such as correlation function and magnetization densities) are invariant under conformal transformations.

In the actual calculation we have calculated the density of points of different type of clusters (crossing clusters, clusters which touch one boundary of the strip, etc.) in analogy with a related study of percolation in [14]. The densities close to free surfaces are well described by scaling predictions, and from this analysis accurate estimate of the critical exponent $x_s-x_b$ is obtained in agreement with the conjecture in Eq. (4). As far as the full profiles are considered, they are well described by the conformal continuum predictions at least for lengths which are larger than the breaking-up length $l_b$. Consequently, our study has given support to the possible validity of the conjectured results.

The second model we considered is the RTFIC, which is a quantum spin chain with quenched disorder and its fixed point is expected to control the critical behavior of a large class of 2D classical systems with anisotropic randomness. Examples are the Ising model and the (directed) percolation with layered disorder. In these systems scaling at the critical point is strongly anisotropic; therefore these systems are not conformally invariant. The RTFIC is studied by the strong-disorder RG method: a finite chain is decimated until a renormalized site, which in terms of the original variables contains some nondecimated sites, which are used to define the final cluster. We have analyzed the density of final clusters, which is shown to obey scaling relations close to the surfaces of the strip. We also tried to find analytical formulas that correctly approximate the numerical profiles. These formulas, which are borrowed from similar studies of conformal systems, have a very good description overall, but they are not fully perfect. We have noticed a discrepancy of the order of a few percent.

Our investigations can be extended in different directions. For 2D classical systems one can study the density of FK clusters in the $q$-state Potts model, both without disorder (for $q \leqslant 4$) and in the presence of disorder (for general values of $q$), and one can consider other types of geometries (semi-infinite strip, square, etc.) as well. One can also study the density of geometrical clusters in the 2D random field Ising model [51,52]. For the random transverse-field Ising model, one possibility is to investigate the distribution of final clusters in a 2D strip.

## ACKNOWLEDGMENTS

We thank L. Turban for useful discussions. This work has been supported by the National Office of Research and Technology under Grant No. ASEP1111, by German-Hungarian exchange programs (DAAD-MÖB and DFG-MTA), and by the Hungarian National Research Fund under OTKA Grants No. TO48721, No. K62588, No. K75324, and No. MO45596. M.K. thanks the Ministère Français des Affaires Étrangères for support.

[1] See, for example, D. Stauffer and A. Aharony, *Introduction to Percolation Theory* (Taylor and Francis, London, 1992).
[2] M. E. Fisher, Physics (Long Island City, N.Y.) **3**, 25 (1967).
[3] A. L. Stella and C. Vanderzande, Phys. Rev. Lett. **62**, 1067 (1989); B. Duplantier and H. Saleur, *ibid.* **63**, 2536 (1989); C. Vanderzande, J. Phys. A **25**, L75 (1992); W. Janke and A. M. J. Schakel, Nucl. Phys. B **700**, 385 (2004).
[4] P. W. Kasteleyn and C. M. Fortuin, J. Phys. Soc. Jpn. **26**, 11 (1969).
[5] J. L. Cardy, J. Phys. A **25**, L201 (1992).
[6] R. M. Ziff, Phys. Rev. Lett. **69**, 2670 (1992).
[7] R. P. Langlands, C. Pichet, Ph. Pouliot, and Y. Saint-Aubin, J. Stat. Phys. **67**, 553 (1992).
[8] M. Aizenman, in *Mathematics of Multiscale Materials*, edited by K. Golden, G. Grimmett, R. James, G. Milton, and P. Sen, IMA Volumes in Mathematics and its Applications (Springer, Berlin, 1998).
[9] P. Kleban and R. M. Ziff, Phys. Rev. B **57**, R8075 (1998).
[10] S. Smirnov, C. R. Acad. Sci., Ser. I: Math. **333**, 239 (2001).
[11] B. Duplantier, J. Stat. Phys. **110**, 691 (2003).
[12] P. Kleban and Don Zagier, J. Stat. Phys. **113**, 431 (2003).
[13] J. Dubédat, Probab. Theory Relat. Fields **134**, 453 (2006).
[14] J. J. H. Simmons, P. Kleban, K. Dahlberg, and R. M. Ziff, J. Stat. Mech.: Theory Exp. (2007) P06012.
[15] T. W. Burkhardt and E. Eisenriegler, J. Phys. A **18**, L83 (1985).
[16] T. W. Burkhardt and J. L. Cardy, J. Phys. A **20**, L233 (1987).
[17] T. W. Burkhardt and I. Guim, Phys. Rev. B **36**, 2080 (1987).
[18] J. L. Cardy, Phys. Rev. Lett. **65**, 1443 (1990).
[19] T. W. Burkhardt and T. Xue, Phys. Rev. Lett. **66**, 895 (1991).
[20] T. W. Burkhardt and T. Xue, Nucl. Phys. B **354**, 653 (1991).
[21] T. W. Burkhardt and E. Eisenriegler, Nucl. Phys. B **424**, 487 (1994).
[22] L. Turban and F. Iglói, J. Phys. A **30**, L105 (1997).
[23] F. Iglói and H. Rieger, Phys. Rev. Lett. **78**, 2473 (1997).
[24] E. Carlon and F. Iglói, Phys. Rev. B **57**, 7877 (1998).
[25] I. Reš and J. P. Straley, Phys. Rev. B **61**, 14425 (2000).
[26] D. Karevski, L. Turban, and F. Iglói, J. Phys. A **33**, 2663 (2000).
[27] U. Bilstein, J. Phys. A **33**, 7661 (2000).
[28] M. Krech, Phys. Rev. B **62**, 6360 (2000).
[29] L. Turban, J. Phys. A **34**, L519 (2001).
[30] For a review, see J. Cardy, Physica A **263**, 215 (1999).
[31] M. Picco, Phys. Rev. Lett. **79**, 2998 (1997); C. Chatelain and B. Berche, *ibid.* **80**, 1670 (1998); Phys. Rev. E **58**, R6899 (1998); **60**, 3853 (1999); T. Olson and A. P. Young, Phys. Rev. B **60**, 3428 (1999).
[32] J. Cardy and J. L. Jacobsen, Phys. Rev. Lett. **79**, 4063 (1997); J. L. Jacobsen and J. Cardy, Nucl. Phys. B **515**, 701 (1998).
[33] B. M. McCoy and T. T. Wu, Phys. Rev. **176**, 631 (1968); **188**, 982 (1969); B. M. McCoy, *ibid.* **188**, 1014 (1969).
[34] D. S. Fisher, Phys. Rev. Lett. **69**, 534 (1992); Phys. Rev. B **51**, 6411 (1995).
[35] For a review, see F. Iglói and C. Monthus, Phys. Rep. **412**, 277 (2005).
[36] T. Senthil and S. N. Majumdar, Phys. Rev. Lett. **76**, 3001 (1996).
[37] R. Juhász and F. Iglói, Phys. Rev. E **66**, 056113 (2002).
[38] J. Hooyberghs, F. Iglói, and C. Vanderzande, Phys. Rev. Lett. **90**, 100601 (2003); Phys. Rev. E **69**, 066140 (2004).
[39] R. Juhász, H. Rieger, and F. Iglói, Phys. Rev. E **64**, 056122 (2001).
[40] J.-Ch. Anglès d'Auriac *et al.*, J. Phys. A **35**, 6973 (2002); J.-Ch. Anglès d'Auriac, in *New Optimization Algorithms in Physics*, edited by A. K. Hartmann and H. Rieger (Wiley-VCH, Berlin, 2004).
[41] J.-Ch. Anglès d'Auriac and F. Iglói, Phys. Rev. Lett. **90**, 190601 (2003).

[42] M. T. Mercaldo, J.-Ch. Anglés d'Auriac, and F. Iglói, Phys. Rev. E **69**, 056112 (2004).
[43] F. Y. Wu, Rev. Mod. Phys. **54**, 235 (1982).
[44] R. J. Baxter, J. Phys. C **6**, L445 (1973).
[45] M. Aizenman and J. Wehr, Phys. Rev. Lett. **62**, 2503 (1989); **64**, 1311(E) (1990).
[46] Y. Imry and M. Wortis, Phys. Rev. B **19**, 3580 (1979); K. Hui and A. N. Berker, Phys. Rev. Lett. **62**, 2507 (1989).
[47] W. Kinzel and E. Domany, Phys. Rev. B **23**, 3421 (1981).
[48] M. E. Fisher and P. G. de Gennes, C. R. Seances Acad. Sci., Ser. B **287**, 207 (1978).
[49] J. Kogut, Rev. Mod. Phys. **51**, 659 (1979).
[50] S. K. Ma, C. Dasgupta, and C.-K. Hu, Phys. Rev. Lett. **43**, 1434 (1979); C. Dasgupta and S. K. Ma, Phys. Rev. B **22**, 1305 (1980).
[51] E. T. Seppälä and M. J. Alava, Phys. Rev. E **63**, 066109 (2001).
[52] L. Környei and F. Iglói, Phys. Rev. E **75**, 011131 (2007).